

Stochastic resolution of identity to CC2 for large systems: Excited-state gradients and derivative couplings

Chongxiao Zhao^{1,2,a)}, Chenyang Li^{3,b),*}, and Wenjie Dou^{1,2,b),*}

1. Department of Chemistry, School of Science, Westlake University, Hangzhou, Zhejiang 310024, China

2. Institute of Natural Sciences, Westlake Institute for Advanced Study, Hangzhou, Zhejiang 310024, China

3. Key Laboratory of Theoretical and Computational Photochemistry, Ministry of Education, College of Chemistry, Beijing Normal University, Beijing 100875, China

^{a)}Email: zhaochongxiao@westlake.edu.cn

^{b)}Authors to whom correspondence should be addressed: chenyang.li@bnu.edu.cn and douwenjie@westlake.edu.cn

Abstract

Excited-state gradients and derivative couplings are critical for simulating excited-state dynamics. However, their calculations are very expensive within the coupled-cluster framework due to the steep scaling. In this work, we present two implementations of stochastic resolution of identity to CC2 (sRI-CC2) for excited-state analytical gradients and derivative couplings. The first method employs sRI for both Coulomb and exchange terms, reducing the formal scaling to cubic. However, this method has a significant stochastic noise. Consequently, we introduce a substitute, termed partial sRI-CC2, which applies sRI selectively to the exchange terms only. The partial sRI-CC2 shows a quartic scaling with a modest prefactor, rendering it a practical alternative. Compared to conventional RI-CC2, the partial sRI-CC2 can handle systems with hundreds or even thousands of electrons. This work is an extension to our previous implementation of sRI-CC2 method and provides essential ingredients for large-scale nonadiabatic dynamics.

I. INTRODUCTION

Over the past decades, the CC2 model has been a well-established method for the accurate calculation of electronic structure properties. The integration of various techniques, such as pair natural orbital (PNO) approach,^[1–5]

local correlation approximation,^[6–9] tensor hypercontraction (THC),^[10–15] spin-component scaling (SCS)^[16–18] and scaled opposite-spin (SOS) modifications,^[14, 19, 20] and others, significantly reduces the original fifth-order computational cost of CC2 and substantially broadens the applicability of CC2 to larger molecular systems. However, most improvements yield only an order of magnitude reduction and a smaller prefactor. Consequently, the application of CC2 to very large systems remains a significant computational challenge.

Among the potential approximation methods, a stochastic variant of resolution of identity (sRI) presents a compelling option. Based on the prevalent RI approach,^[21–23] this technique employs randomly generated stochastic orbitals to further decouple the four-index electron repulsion integrals (ERIs). Combined with Laplace transform,^[24–26] the sRI approximation is very efficient in evaluating MP2-energy-like intermediates, which is ubiquitous in common electronic structure methods. Therefore, the sRI technique gains rapid popularity in many implementations, such as DFT,^[27–31] MP2,^[32–34] GF2^[35–39] and etc.^[40, 41] Recently, we introduce sRI to CC2 ground and excited-state energy,^[42, 43] oscillator strength and ground-state analytical gradient,^[44] achieving a steep scaling reduction from $O(N^5)$ to $O(N^3)$ or $O(N^4)$. This reduced computational cost enables CC2 calculations on systems with hundreds or even thousands of electrons. To complete the sRI-CC2 series and facilitate its application in dynamics simulations, the next step falls on excited-state analytical gradients and derivative couplings.

The analytical energy derivative of excited states is essential for determining equilibrium geometries and conducting molecular dynamics simulations. The explicit formulations of CC2 excited-state gradient were first reported by Hättig *et al.*^[45, 46] Afterwards, several improvements were carried out.^[47–49] The derivative coupling is also critical for dynamics simulations, and the CC2 method represents a promising approach for their calculation. However, the situation of CC2 derivative couplings is more complex, and their feasibility was a subject of debate two decades ago.^[50, 51] Due to the lack of Hermitian symmetry, conical intersections between states spanning the same symmetry would encounter complex energy and result in a defective intersection. This challenge was recently addressed by Koch *et al.* through the development of a modified CC2 theory, termed similarity constrained CC2 (SCC2).^[52–54] Their approach is demonstrated to correctly describe conical intersections within the coupled cluster framework.^[55–57]

CC2 has been implemented in various software packages including Psi4,^[58] COLUMBUS,^[59] Pyscf,^[60]. This work is mainly developed using the Q-Chem package^[61–64] and presents two implementations of sRI-CC2 for the computation of excited-state analytical gradients and derivative couplings. The first, designated the complete sRI-CC2 method, is implemented with cubic scaling. However, its practical application is severely constrained by the requirement for a large number of stochastic orbitals. To overcome this limitation, we introduce a quartic-scaling variant, termed partial sRI-CC2, which employs sRI selectively within the exchange terms. This partial implementation demonstrates superior accuracy and its reduced scaling enables the calculations of systems with hun-

dreds or even thousands of electrons.

This paper is organized as follows: In Sec. II, we present the theoretical framework and detailed algorithms for excited-state analytical gradient and derivative coupling at the sRI-CC2 level. This section also examines the differences between RI and sRI approximations and outlines the justification for our partial sRI-CC2. Sec. III evaluates the numerical accuracy of the sRI-CC2 method and compares its computational cost to the RI-CC2 method. Sec. IV gives a conclusion.

II. THEORY

The notation defined in Table I is used throughout this work. All values in the final column scale proportionally with the system size N .

Table I: Summary of notations in the following equations.

Item	Function or indices	Total number
AO Gaussian basis functions	$\chi_\alpha(r_1), \chi_\beta(r_1), \chi_\gamma(r_1), \chi_\delta(r_1), \dots$	N_{AO}
Auxiliary basis functions	P, Q, R, S, \dots	N_{aux}
General sets of AOs	$\alpha, \beta, \gamma, \delta, \dots$	N_{ao}
General sets of MOs	p, q, r, s, \dots	N_{mo}
Occupied (active) MOs	i, j, k, l, \dots	N_{occ}
Unoccupied (virtual) MOs	a, b, c, d, \dots	N_{vir}

A. CC2 theory

In the CC2 formulation,^[65] the T_1 -transformed Hamiltonian \hat{H} provides a convenient framework

$$\hat{H} = e^{-T_1} H e^{T_1} \quad (1)$$

The cluster operators $T_n = \sum_{\mu_n} t_{\mu_n} \tau_{\mu_n}$ consist of the cluster amplitudes $t_{\mu_n} = t_{ij\dots}^{ab\dots}$ and the excitation operators $\tau_{\mu_n} = E_{ai} E_{bj} \dots$. As an approximation to the CCSD model, the CC2 model only involves the singly and doubly excited cluster operators.

The left-projection of the Hartree-Fock wave function $|HF\rangle$ and excitation determinant $|\mu_i\rangle = \tau_{\mu_i} |HF\rangle$ onto the CC2 Schrödinger equation generates the complete set of equations for the CC2 ground-state energy and amplitudes.

$$E_{CC2} = \langle HF | \hat{H} + [\hat{H}, T_2] | HF \rangle \quad (2)$$

$$\Omega_{\mu_1} = \langle \mu_1 | \hat{H} + [\hat{H}, T_2] | HF \rangle = 0 \quad (3)$$

$$\Omega_{\mu_2} = \langle \mu_2 | \hat{H} + [F, T_2] | HF \rangle = 0 \quad (4)$$

Here E_{CC2} is the CC2 ground-state energy and the residuals $\Omega_{\mu_i}, i = 1, 2$ are termed CC vector functions. F is the Fock operator.

Two equivalent approaches are available for computing excitation energies within the CC2 framework. The first, known as the linear response (LR) theory,^[66–68] obtains them by solving the eigenvalue equation associated with the unsymmetric Jacobian matrix \mathbf{A} of the vector function Ω_{μ_i}

$$A_{\mu_i\nu_j} = \frac{\partial\Omega_{\mu_i}}{\partial t_{\nu_j}} = \begin{pmatrix} \langle\mu_1|[\hat{H}, \tau_{\nu_1}] + [[\hat{H}, \tau_{\nu_1}], T_2]|HF\rangle & \langle\mu_1|[\hat{H}, \tau_{\nu_2}]|HF\rangle \\ \langle\mu_2|[\hat{H}, \tau_{\nu_1}]|HF\rangle & \delta_{\mu_2\nu_2}\epsilon_{\mu_2} \end{pmatrix} \quad (5)$$

The doubles-doubles block is diagonal with the orbital energy difference ϵ_{μ_2}

$$\epsilon_{\mu_2} = \epsilon_{aibj} = \epsilon_a - \epsilon_i + \epsilon_b - \epsilon_j \quad (6)$$

so the eigenvalue equation of the Jacobian can be solved with the effective singles-singles block $A_{\mu_1\nu_1}^{eff}$

$$A_{\mu_1\nu_1}^{eff} = A_{\mu_1\nu_1} - \frac{A_{\mu_1\gamma_2}A_{\gamma_2\nu_1}}{\epsilon_{\gamma_2} - \omega} \quad (7)$$

Solutions from the right and the left respectively give the right (r_{μ_1}) and left (l_{μ_1}) eigenvectors with the same excitation energy ω .

$$A_{\mu_1\nu_1}^{eff}(\omega)r_{\nu_1} = \omega r_{\mu_1} \quad (8)$$

$$l_{\mu_1}A_{\mu_1\nu_1}^{eff}(\omega) = \omega l_{\nu_1} \quad (9)$$

Another approach is the equation-of-motion (EOM) formulation.^[13, 69–74] The wave function for the m -th excited state is constructed by applying a linear excitation operator R_m to the CC2 ground-state wave function.

$$|\psi_m\rangle = R_m|\psi_0\rangle \quad (10)$$

$$R_m = r_0^m + R_1^m + R_2^m = r_0^m + \sum_{i=1}^2 r_{\mu_i}^m \tau_{\mu_i} \quad (11)$$

After a sequence of transformations, the final EOM-CC2 equation is derived

$$[\bar{H}_N, R_m]|HF\rangle = \omega_m R_m|HF\rangle \quad (12)$$

The normal-ordered T_1 -transformed Hamiltonian is defined as

$$\bar{H}_N = e^{-T_1} H e^{T_1} - \langle HF|e^{-T_1} H e^{T_1}|HF\rangle \quad (13)$$

$$(\bar{H}_N)_{\mu_i\nu_j} = \begin{pmatrix} 0 & \langle HF|\bar{H}_N|\nu_1\rangle & \langle HF|\bar{H}_N|\nu_2\rangle \\ 0 & \langle\mu_1|\bar{H}_N|\nu_1\rangle & \langle\mu_1|\bar{H}_N|\nu_2\rangle \\ 0 & \langle\mu_2|\bar{H}_N|\nu_1\rangle & \langle\mu_2|\bar{H}_N|\nu_2\rangle \end{pmatrix} \quad (14)$$

The two-by-two block in the lower right corner is equivalent to the Jacobian in the LR theory, and thus gives the same excitation energy.

Due to the non-Hermitian properties of \bar{H}_N , solving the eigenvalue problem from the left side also yields a set of intermediates

$$L_m = L_1^m + L_2^m = \sum_{i=1}^2 l_{\mu_i}^m \tau_{\mu_i} \quad (15)$$

The right and left eigenvectors are biorthonormal and the excitation energy is given as

$$\langle HF | L_m R_n | HF \rangle = \delta_{mn} \quad (16)$$

$$\omega_m = \langle HF | L_m [\bar{H}_N, R_m] | HF \rangle \quad (17)$$

B. CC2 excited-state analytical gradient

The analytical gradient formulation for CC2 excited states, using the Lagrange approach,^[75, 76] parallels that of the ground state.^[44, 45, 77, 78]

$$\begin{aligned} L = E_{CC2} &+ \sum_{\mu\nu} l_{\mu} A_{\mu\nu} r_{\nu} + \bar{\omega} \left(1 - \sum_{\mu} l_{\mu} r_{\mu} \right) \\ &+ \sum_{\mu} \bar{t}_{\mu} \Omega_{\mu} + \sum_{pq} \zeta_{pq} (F_{pq} - \delta_{pq} \varepsilon_p) + \sum_{pq} \omega_{pq} (S_{pq} - \delta_{pq}) \end{aligned} \quad (18)$$

The total energy of the target excited state is given by the sum of the CC2 ground-state energy (E_{CC2}) and the excitation energy, represented by the first and second terms, respectively. The third term ensures the biorthonormality of the excitation amplitudes, while the fourth term constrains the ground-state amplitudes. The final two terms arise from the use of a Hartree-Fock reference and encapsulate the orbital relaxation contributions.

Subsequently, the key point of the problem lies in solving for the four Lagrange multipliers, $\bar{\omega}$, \bar{t}_{μ} , ζ_{pq} and ω_{pq} . Varying the Lagrangian with respect to l_{μ} or r_{μ} yields $\bar{\omega} = \omega$.

$$\frac{\partial L}{\partial l_{\mu}} = \sum_{\nu} A_{\mu\nu} r_{\nu} - \bar{\omega} r_{\mu} = 0 \quad (19)$$

$$\frac{\partial L}{\partial r_{\nu}} = \sum_{\mu} l_{\mu} A_{\mu\nu} - \bar{\omega} l_{\nu} = 0 \quad (20)$$

The detailed solution for \bar{t}_{μ} was derived by Hättig *et al.*^[79] through differentiation of the Lagrangian L with respect to t_{μ}

$$\frac{\partial L}{\partial t_{\nu}} = \frac{\partial E_{CC2}}{\partial t_{\nu}} + \sum_{\mu\gamma} l_{\mu} \frac{A_{\mu\gamma}}{t_{\nu}} r_{\gamma} + \sum_{\mu} \bar{t}_{\mu} \frac{\Omega_{\mu}}{t_{\nu}} = 0 \quad (21)$$

Defining

$$\eta_\nu = \frac{\partial E_{CC2}}{\partial t_\nu} \quad (22)$$

$$B_{\mu\gamma\nu} = \frac{\partial A_{\mu\gamma}}{\partial t_\nu} \quad (23)$$

and then Eq. (21) can be rewritten as

$$\sum_\mu t_\mu \bar{A}_{\mu\nu} = - \left(\eta_\nu + \sum_{\mu\gamma} l_\mu B_{\mu\nu\gamma} r_\gamma \right) \quad (24)$$

The rest two Lagrange multipliers ζ_{pq} and ω_{pq} are derived from the variational condition with respect to the MO coefficients C

$$\frac{\partial L}{\partial C_{\mu q}} = 0 \quad (25)$$

which is known as Z-vector equation.^[80–82] The two indices μ and p are defined in AO basis and MO basis, respectively. For consistency, the index μ is transformed back to the MO basis through^[45, 77]

$$\sum_\mu C_{\mu p} \frac{\partial L}{\partial C_{\mu q}} = 0 \quad (26)$$

Using the unrelaxed one- ($\bar{\gamma}_{pq}$) and two-body ($\bar{\gamma}_{rs}^{pq}$) reduced density matrices (RDMs) (see Appendix), the CC2 Lagrangian can be expressed in a compact form

$$L = \sum_{pq} \bar{\gamma}_{pq} h_{pq} + \sum_{pqrs} \bar{\gamma}_{rs}^{pq} (pq|rs) + \sum_{pq} \zeta_{pq} (F_{pq} - \delta_{pq} \varepsilon_p) + \sum_{pq} \omega_{pq} (S_{pq} - \delta_{pq}) \quad (27)$$

with h_{pq} and $(pq|rs)$ being the one- and two-electron integrals, respectively.

The first derivative of Lagrangian with respect to the nuclear coordinates x , the analytical gradient, is constructed as

$$\frac{\partial L}{\partial x} = \sum_{pq} \gamma_{pq} h_{pq}^{[x]} + \sum_{pqrs} \gamma_{rs}^{pq} (pq|rs)^{[x]} + \sum_{pq} \omega_{pq} S_{pq}^{[x]} \quad (28)$$

The superscript $[x]$ indicates the first derivative with respect to x . The orbital response contributions are incorporated in the final one- (γ_{pq}) and two-PDMs (γ_{rs}^{pq})

$$\gamma_{pq} \leftarrow \bar{\gamma}_{pq} \quad (29)$$

$$\gamma_{ia} \leftarrow \zeta_{ai} \quad (30)$$

$$\gamma_{rs}^{pq} \leftarrow \bar{\gamma}_{rs}^{pq} \quad (31)$$

$$\gamma_{ak}^{ik} \leftarrow \zeta_{ai} \quad (32)$$

C. CC2 derivative coupling

The Lagrangian for the derivative coupling^[53] between states m and n is analogous to that of the gradient.

$$L_{mn} = \mathcal{O}_{mn} + \sum_{\mu} \bar{\gamma}_{\mu} \left(\sum_{\nu} A_{\mu\nu} r_{\nu}^n - \omega_n r_{\mu}^n \right) + \bar{\omega} \left(1 - \sum_{\mu} l_{\mu}^n r_{\mu}^n \right) + \sum_{\mu} \bar{t}_{\mu} \Omega_{\mu} + \sum_{pq} \zeta_{pq} (F_{pq} - \delta_{pq} \varepsilon_p) + \sum_{pq} \omega_{pq} (S_{pq} - \delta_{pq}) \quad (33)$$

Here, the first term is defined as

$$\mathcal{O}_{mn} = \langle \psi_m^L(x_0) | \psi_n^R(x) \rangle \quad (34)$$

The nuclear coordinate of the left state m is fixed at x_0 and any derivative acts only on the right state n with a varying x . For notational convenience, the dependence on x_0 and x is suppressed in Eq. (33). And the derivative of L_{mn} with respect to x at x_0 appears as

$$F_{mn}(x_0) \equiv \frac{d\mathcal{O}_{mn}}{dx} \Big|_{x=x_0} = \left\langle \psi_m^L(x_0) \left| \frac{d}{dx} \psi_n^R(x) \right|_{x=x_0} \right\rangle = \frac{dL_{mn}}{dx} \Big|_{x=x_0} = \frac{\partial L_{mn}}{\partial x} \Big|_{x=x_0} \quad (35)$$

The second term specifies the excited-state amplitudes. The n -excited-state energy is given as ω_n

$$\omega_n = \langle L_n | [\bar{H}, R_n] | HF \rangle = \sum_{\mu\nu} l_{\mu}^n A_{\mu\nu} r_{\nu}^n \quad (36)$$

$$\bar{H} = e^{-T_2 - T_1} H e^{T_1 + T_2} \quad (37)$$

The remaining four constraints fulfill an analogous function to those defined in the gradient section.

Still, we need to solve the Lagrange multipliers $\bar{\gamma}_{\mu}$, $\bar{\omega}$, \bar{t}_{μ} , ζ_{pq} and ω_{pq} first. The stationarity for r_{μ}^n is

$$\frac{\partial L_{mn}}{\partial r_{\sigma}^n} = l_{\sigma}^m + \sum_{\mu} \bar{\gamma}_{\mu} A_{\mu\sigma} - \omega_n \bar{\gamma}_{\sigma} - \sum_{\mu} \omega_n \bar{\gamma}_{\mu} r_{\mu}^n l_{\sigma}^n - \bar{\omega} l_{\sigma}^n = 0 \quad (38)$$

and this yields $\bar{\gamma}_{\mu}$ and $\bar{\omega}$

$$\bar{\gamma}^T = \frac{\mathbf{l}_m^T}{\omega_n - \omega_m} \quad (39)$$

$$\bar{\omega} = -\omega_n \bar{\gamma}^T \mathbf{r}_n \quad (40)$$

The stationarity for t_{μ} reads

$$\frac{\partial L_{mn}}{\partial t_{\sigma}} = l_{\sigma}^m r_0^n + \delta_{\sigma, ai} \sum_{bj} l_{aibj}^m r_{bj}^n + \sum_{\mu\nu} \bar{\gamma}_{\mu} r_{\nu}^n B_{\mu\nu\sigma} + \sum_{\mu\sigma} \bar{t}_{\mu} A_{\mu\sigma} = 0 \quad (41)$$

The initial two terms on the right side of the equation are independent of $\bar{\gamma}_\mu$ and the solution follows an analogous procedure to the gradient scheme. The remaining two multipliers are solved through Z-vector equation, as detailed in Eq. (26). The additional contributions arising from \mathcal{O}_{mn} addressed separately. The explicit expressions for the unrelaxed RDMs can be found in the Appendix. The specific contribution of \mathcal{O}_{mn} to the Z-vector equation is as follows

$$\sum_{\mu} C_{\mu p} \frac{\partial \mathcal{O}_{mn}}{\partial C_{\mu q}} \Big|_{x=x_0} = \sum_{\mu} C_{\mu p} \frac{\partial \langle L_m | e^{-T} e^T | R_n \rangle \Big|_{x=x_0}}{\partial C_{\mu q}} \quad (42)$$

$$= \bar{\gamma}_{pq} (l_\mu^m, R_\nu^n) \quad (43)$$

which equals the 1-RDM from LAR terms. Its derivative with respect to the nuclear coordinates reads

$$\frac{\partial \mathcal{O}_{mn}}{\partial x} \Big|_{x=x_0} = \sum_{pq} \bar{\gamma}_{pq}^{mn} \langle \psi_p | \psi_q^{[x]} \rangle \quad (44)$$

$$S_{pq}^{R[x]} = \langle \psi_p | \psi_q^{[x]} \rangle \quad (45)$$

The overlap derivatives are not symmetric, and here the right derivative $S_{pq}^{R[x]}$ is available in packages like Psi4,^[58] Q-Chem,^[61] etc.

D. sRI approximation and Laplace transform

The RI technique adopts a set of auxiliary basis functions to decouple the four-index ERIs

$$(\alpha\beta|\gamma\delta) \approx \sum_{PR} (\alpha\beta|P) [V^{-1}]_{PR} (R|\gamma\delta) \quad (46)$$

$$= \sum_Q \left[\sum_P (\alpha\beta|P) V_{PQ}^{-1/2} \right] \left[\sum_R V_{QR}^{-1/2} (R|\gamma\delta) \right] \quad (47)$$

$$= \sum_Q B_{\alpha\beta}^Q B_{\gamma\delta}^Q \quad (48)$$

The three-index RI tensor $B_{\alpha\beta}^Q$ is given as

$$B_{\alpha\beta}^Q = \sum_P (\alpha\beta|P) V_{PQ}^{-1/2} \quad (49)$$

The stochastic RI, abbreviated as sRI, introduces an additional set of stochastic orbitals to further decouple the four-index ERIs.^[34] Each element of these stochastic orbitals $\{\theta^\xi\}$, $\xi = 1, 2, \dots, N_s$, is randomly generated to be 1 or -1 and they exhibit the following property.

$$\langle \theta \otimes \theta \rangle_\xi = \frac{1}{N_s} \sum_{\xi=1}^{N_s} \theta^\xi \otimes (\theta^\xi)^T \approx I \quad (50)$$

The number of these stochastic orbitals N_s , different from N_{aux} , is independent of the system size, and this will be discussed further in a subsequent section. By inserting the $\langle \theta \otimes \theta \rangle_\xi$ in the right foremost of Eq. (48), the sRI realization of four-index ERI is expressed as

$$\begin{aligned}
(\alpha\beta|\gamma\delta) &\approx \sum_{QS} \sum_{PR} (\alpha\beta|P) V_{PQ}^{-1/2} \left(\langle \theta \otimes \theta^T \rangle_\xi \right)_{QS} V_{SR}^{-1/2} (R|\gamma\delta) \\
&= \left\langle \sum_P \left[(\alpha\beta|P) \sum_Q \left(V_{PQ}^{-1/2} \theta_Q \right) \right] \sum_R \left[(R|\gamma\delta) \sum_S \left(V_{SR}^{-1/2} \theta_S \right) \right] \right\rangle_\xi \quad (51) \\
&= \left\langle R_{\alpha\beta}^\xi R_{\gamma\delta}^\xi \right\rangle_\xi = \frac{1}{N_s} \sum_{\xi=1}^{N_s} R_{\alpha\beta}^\xi R_{\gamma\delta}^\xi
\end{aligned}$$

The sRI tensor $R_{\alpha\beta}^\xi$ contains two indices in AO basis, α and β , and the original size-dependent index Q in the RI tensor is replaced by a size-independent one ξ . This formulation allows $R_{\alpha\beta}^\xi$ to be treated as a two-rank tensor. Also, the computational cost of four-index ERIs is reduced from $O(N_{aux}N_{AO}^4)$ to $O(N_sN_{AO}^4)$, where the constant prefactor N_s is conventionally neglected.

In practice, the sRI approximation to four-index ERIs is always combined with the Laplace transform for the evaluation of MP2 energy-like terms, for example,

$$\begin{aligned}
\frac{(ai|bj)}{\epsilon_i - \epsilon_a + \epsilon_j - \epsilon_b} &= - \int_0^\infty \left\langle R_{ai}^\xi R_{bj}^\xi \right\rangle_\xi e^{(\epsilon_i - \epsilon_a + \epsilon_j - \epsilon_b)t} dt \\
&\approx - \sum_z^{N_z} w_z \left[\left\langle R_{ai}^\xi R_{bj}^\xi \right\rangle_\xi e^{(\epsilon_i - \epsilon_a)t_z} e^{(\epsilon_j - \epsilon_b)t_z} \right] \\
&= - \sum_z^{N_z} w_z \left\langle \left[R_{ai}^\xi e^{(\epsilon_i - \epsilon_a)t_z} \right] \left[R_{bj}^\xi e^{(\epsilon_j - \epsilon_b)t_z} \right] \right\rangle_\xi \quad (52) \\
&= - \sum_z^{N_z} w_z \left\langle N_{ai}^{R,\xi} N_{bj}^{R,\xi} \right\rangle_\xi
\end{aligned}$$

The orbital energy denominator is decoupled into the exponential forms $e^{(\epsilon_i - \epsilon_a)t_z}$. Combined with the sRI tensor R_{ai}^ξ , it is contracted into $N_{ai}^{R,\xi}$.

$$N_{ai}^{R,\xi} = R_{ai}^\xi e^{(\epsilon_i - \epsilon_a)t_z} \quad (53)$$

The superscript R indicates the origin of this intermediate and is not an index in the final scaling. Due to the variety of four-index electron repulsion integral (ERI) expressions within the CC2 formalism, analogous cases will subsequently be introduced using this notation. The variables w_z and t_z denotes the weights and grid points of the numerical quadrature, respectively. The N_z is the number of these quadrature points and a value of $N_z = 7$ is selected for modest accuracy. N_z is also independent of the system size, resulting only in an increased prefactor for the computational scaling.

E. Details of sRI-CC2 formulations

The mathematical formalism for the CC2 excited-state gradient closely parallels that of the derivative coupling. Analogous to the CC2 energy calculation, their time-determining steps lie in the tensor contractions of double amplitudes with four-index ERIs (both usually appear in modified forms), for example,

$$\begin{aligned}
\sum_{abj} \hat{t}_{ij}^{ab}(bj|ak) &= \sum_{PQabj} \frac{2\hat{B}_{ai}^P \hat{B}_{bj}^P - \hat{B}_{bi}^P \hat{B}_{aj}^P}{\epsilon_i - \epsilon_a + \epsilon_j - \epsilon_b} B_{bj}^Q B_{ak}^Q \\
&= - \sum_z^{N_z} w_z \sum_{PQabj} \left(2N_{ai}^{\hat{B},P} N_{bj}^{\hat{B},P} - N_{bi}^{\hat{B},P} N_{aj}^{\hat{B},P} \right) B_{bj}^Q B_{ak}^Q \\
&= - \sum_z^{N_z} w_z \sum_{PQabj} \left[2 \left(N_{bj}^{\hat{B},P} B_{bj}^Q \right) N_{ai}^{\hat{B},P} - \left(N_{bi}^{\hat{B},P} B_{bj}^Q \right) N_{aj}^{\hat{B},P} \right] B_{ak}^Q
\end{aligned} \tag{54}$$

In the preceding equation, the expression is reformulated using RI and Laplace transform, leading to a decomposition into a tensor contraction of the three-index RI matrix \hat{B}_{ai}^P with its Laplace-transformed version

$$N_{ai}^{\hat{B},P} = \hat{B}_{ai}^P e^{(\epsilon_i - \epsilon_a)t_z} \tag{55}$$

This process employs a strategy of canceling identical indices to achieve a lower computational cost. The procedure exhibits an asymptotic scaling of $O(N^5)$, dominated by the exchange term, while the Coulomb term scales as $O(N^4)$. A detailed cost analysis for each step, including a comparison with sRI version, is provided in Table II.

The application of sRI approximation to all four-index ERIs in Eq. (54), which we refer to as complete sRI, reduces the computational scaling of both the Coulomb and exchange terms to $O(N^3)$.

$$\begin{aligned}
\sum_{abj} \hat{t}_{ij}^{ab}(bj|ak) &= \sum_{abj} \frac{2\langle \hat{R}_{ai}^{\xi'} \hat{R}_{bj}^{\xi'} \rangle_{\xi'} - \langle \hat{R}_{bi}^{\xi'} \hat{R}_{aj}^{\xi'} \rangle_{\xi'}}{\epsilon_i - \epsilon_a + \epsilon_j - \epsilon_b} \langle R_{bj}^{\xi} R_{ak}^{\xi} \rangle_{\xi} \\
&= - \left\langle \sum_z^{N_z} w_z \sum_{abj} \left(2N_{ai}^{\hat{R},\xi'} N_{bj}^{\hat{R},\xi'} - N_{bi}^{\hat{R},\xi'} N_{aj}^{\hat{R},\xi'} \right) R_{bj}^{\xi} R_{ak}^{\xi} \right\rangle_{\xi\xi'} \\
&= - \left\langle \sum_z^{N_z} w_z \sum_{abj} \left[2 \left(N_{bj}^{\hat{R},\xi'} R_{bj}^{\xi} \right) N_{ai}^{\hat{R},\xi'} - \left(N_{bi}^{\hat{R},\xi'} R_{bj}^{\xi} \right) N_{aj}^{\hat{R},\xi'} \right] R_{ak}^{\xi} \right\rangle_{\xi\xi'}
\end{aligned} \tag{56}$$

$$N_{ai}^{\hat{R},\xi'} = \hat{R}_{ai}^{\xi'} e^{(\epsilon_i - \epsilon_a)t_z} \tag{57}$$

Two sets of stochastic orbitals $\xi\xi'$ are used because the two four-index ERIs are independent. The use of stochastic samplings introduces a standard deviation (S.D.), which can be mitigated by utilizing more stochastic orbitals. The detailed cost for each step is also shown in Table II.

Our prior study^[44] shows that the complete sRI is not well-suited for the evaluation of gradient-like properties. This inadequacy stems from the considerable statistical uncertainty, particularly from the sRI treatment of the Coulomb integrals, which drastically increases the computational prefactor N_s required for acceptable precision. To mitigate this, we propose a partial sRI scheme that restricts the sRI approximation exclusively to the exchange term in the numerator of the double amplitudes.

$$\sum_{abj} \hat{t}_{ij}^{ab}(bj|ak) = - \sum_z w_z \sum_{abj} \left[2 \left(N_{bj}^{\hat{B},P} B_{bj}^Q \right) N_{ai}^{\hat{B},P} - \langle \left(N_{bi}^{\hat{R},\xi'} B_{bj}^Q \right) N_{aj}^{\hat{R},\xi'} \rangle_{\xi'} \right] B_{ak}^Q \quad (58)$$

The Coulomb term without sRI retains the $O(N^4)$ scaling, while the exchange term with sRI scales as $O(N^4)$ with a discernible loss of accuracy. The prefactor N_s remains manageable. In contrast to the complete sRI, which attains an $O(N^3)$ scaling, the partial sRI formulation achieves an $O(N^4)$ scaling but significantly reduces stochastic errors. An analysis of both partial sRI and complete sRI, based on empirical data, is presented in the subsequent section.

III. RESULTS AND DISCUSSION

In this section, we first assess performance of our sRI-CC2 excited-state gradient and derivative coupling programs in accuracy and cost across a range of molecular systems. Subsequently, we evaluate the required number of stochastic orbitals N_s for two distinct sRI approaches. Our implementation is integrated within the Q-Chem package. All the calculations employ the cc-pVDZ basis set. Given the stochastic nature of the sRI technique, the reported sRI-CC2 results represent an average over ten independent calculations, each initialized with a unique random seed. The corresponding standard deviations are depicted as error bars in the accompanying figures. The sRI-CC2 variant is deemed accurate if the standard deviation is sufficiently small (a parameter controllable via N_s and tuned for the desired precision) and exceeds the systematic error (i.e., the deterministic RI-CC2 result falls within the error bar). Unless otherwise stated, we utilize $N_s = 100$ for the partial sRI-CC2 and $N_s = 50000$ for the complete sRI-CC2. The rationale for these selections is discussed in Subsec. C.

The output of both the gradient and derivative coupling tests is a matrix of dimensions $3 \times N_{natom}$ (where N_{natom} is the number of atoms), complicating direct result comparison. To quantify the overall numerical error, we denote the element-wise error as Δ_i and employ two metrics: the maximum error (Δ_{max}) and the mean absolute error ($\bar{\Delta}_{abs}$)

$$\Delta_{max} = \max_i |\Delta_i| \quad (59)$$

$$\bar{\Delta}_{abs} = \frac{1}{n} \sum_{i=1}^n |\Delta_i| \quad (60)$$

Table II: Details of intermediate steps. The A , C and D in the first column are just intermediates in the calculations. The prefactor N_s in the costs and $\xi\xi'$ in the intermediates are omitted for brevity. ‘0’ in the index means that all the indices are cancelled, only returning a constant. The calculations from C to D for Coulomb and exchange terms can be combined, and here we leave both for completeness.

Coulomb term			Exchange term		
RI					
Term	Index	Cost	Term	Index	Cost
$N_{bj}^{\hat{B},P} B_{bj}^Q \rightarrow A^{PQ}$	$Pbj \times Qbj \rightarrow PQ$	$O(N^4)$	$N_{bi}^{\hat{B},P} B_{bj}^Q \rightarrow A_{ij}^{PQ}$	$Pbi \times Qbj \rightarrow PQij$	$O(N^5)$
$A^{PQ} N_{ai}^{\hat{B},P} \rightarrow C_{ai}^Q$	$PQ \times Pai \rightarrow Qai$	$O(N^4)$	$A_{ij}^{PQ} N_{aj}^{\hat{B},P} \rightarrow C_{ai}^Q$	$PQij \times Paj \rightarrow Qai$	$O(N^5)$
$C_{ai}^Q B_{ak}^Q \rightarrow D_{ik}$	$Qai \times Qak \rightarrow ik$	$O(N^4)$	$C_{ai}^Q B_{ak}^Q \rightarrow D_{ik}$	$Qai \times Qak \rightarrow ik$	$O(N^4)$
Complete sRI					
Term	Index	Cost	Term	Index	Cost
$N_{bj}^{\hat{R},\xi'} R_{bj}^\xi \rightarrow A_0$	$bj \times bj \rightarrow 0$	$O(N^2)$	$N_{bi}^{\hat{R},\xi'} R_{bj}^\xi \rightarrow A_{ij}$	$bi \times bj \rightarrow ij$	$O(N^3)$
$A_0 N_{ai}^{\hat{R},\xi'} \rightarrow C_{ai}$	$0 \times ai \rightarrow ai$	$O(N^2)$	$A_{ij} N_{aj}^{\hat{R},\xi'} \rightarrow C_{ai}$	$ij \times aj \rightarrow ai$	$O(N^3)$
$C_{ai} R_{ak}^\xi \rightarrow D_{ik}$	$ai \times ak \rightarrow ik$	$O(N^3)$	$C_{ai} R_{ak}^\xi \rightarrow D_{ik}$	$ai \times ak \rightarrow ik$	$O(N^3)$
Partial sRI					
Term	Index	Cost	Term	Index	Cost
$N_{bj}^{\hat{B},P} B_{bj}^Q \rightarrow A^{PQ}$	$Pbj \times Qbj \rightarrow PQ$	$O(N^4)$	$N_{bi}^{\hat{R},\xi'} B_{bj}^Q \rightarrow A_{ij}^Q$	$bi \times Qbj \rightarrow Qij$	$O(N^4)$
$A^{PQ} N_{ai}^{\hat{B},P} \rightarrow C_{ai}^Q$	$PQ \times Pai \rightarrow Qai$	$O(N^4)$	$A_{ij}^Q N_{aj}^{\hat{R},\xi'} \rightarrow C_{ai}^Q$	$Qij \times aj \rightarrow Qai$	$O(N^4)$
$C_{ai}^Q B_{ak}^Q \rightarrow D_{ik}$	$Qai \times Qak \rightarrow ik$	$O(N^4)$	$C_{ai}^Q B_{ak}^Q \rightarrow D_{ik}$	$Qai \times Qak \rightarrow ik$	$O(N^4)$

The former gives the largest error and the latter indicates the general magnitude of error. We use these two indicators to measure the errors from our sRI-CC2.

All the calculations are carried out in the high performance computing (HPC) center of Westlake University, utilizing an AMD EPYC 7502 (2.5 GHz) node with 64 computational cores.

A. CC2 excited-state gradient

We initially benchmark the accuracy of our RI-CC2 implementation with the program in turbomole^[45,83]. Subsequently, we assess the validity of our new sRI-CC2 programs across a broader set of molecular systems. As summarized in Table III, we provide the statistical errors for partial sRI-CC2 and complete sRI-CC2 with respect to RI-CC2. For partial sRI-CC2 with $N_s = 100$, all the Δ_{max} for gradient are maintained below 0.01 hartree/bohr, and all the $\bar{\Delta}_{abs}$ below 0.002 hartree/bohr. In contrast, the complete sRI-CC2 method with $N_s = 50000$ exhibits significantly larger statistical fluctuations and its errors for both the gradient and standard deviation are several times greater than those of the partial sRI-CC2. Although these errors can be reduced by increasing the number of stochastic orbitals, the associated computational prefactor becomes prohibitively large for systems containing hundreds of electrons. Consequently, the potential advantage of complete sRI-CC2 with a cubic scaling may be realized in larger systems beyond our test range. In the following sections, we therefore focus our analysis on the performance of the partial sRI-CC2 approach.

Table III: CC2 excited-state gradient error analyses of various systems (in hartree/bohr). The statistical error takes RI-CC2 data as a reference.

Molecule	Partial sRI-CC2				Complete sRI-CC2			
	Gradient		S.D.		Gradient		S.D.	
	Δ_{max}	$\bar{\Delta}_{abs}$	Δ_{max}	$\bar{\Delta}_{abs}$	Δ_{max}	$\bar{\Delta}_{abs}$	Δ_{max}	$\bar{\Delta}_{abs}$
H ₂	0.0006	0.0004	0.0012	0.0010	0.0001	0.0001	0.0024	0.0017
H ₂ O	0.0011	0.0004	0.0049	0.0026	0.0132	0.0054	0.0221	0.0147
HF	0.0031	0.0014	0.0055	0.0030	0.0051	0.0045	0.0236	0.0168
LiH	0.0007	0.0004	0.0007	0.0005	0.0006	0.0003	0.0018	0.0013
LiF	0.0022	0.0009	0.0025	0.0015	0.0019	0.0011	0.0158	0.0085
NH ₃	0.0014	0.0006	0.0037	0.0021	0.0128	0.0057	0.0182	0.0121
Benzene	0.0045	0.0010	0.0050	0.0021	0.1921	0.0303	0.3062	0.0899
Furan	0.0079	0.0016	0.0351	0.0058	0.1145	0.0193	0.1356	0.0565
Pyrrole	0.0030	0.0008	0.0081	0.0025	0.0823	0.0162	0.2340	0.0791
Pyridine	0.0076	0.0014	0.0079	0.0032	0.0819	0.0172	0.2500	0.0789

In Table IV, we exhibit the partial sRI-CC2 results for a series of (all-*E*)-olefin chains. Such series extended systems with similar structures and properties provides a convenient framework for evaluating computational costs and

error estimation. A more direct visualization of the data is also shown in Fig. 1. With the increase of the number of electrons N_e , the two measures retain the value in a stable range and don't show obvious positive correlation trend. This indicates that a value of $N_s = 100$ is sufficient for all these calculations. The stochastic error introduced by sRI does not increase with the system size, eliminating the need to adjust N_s for larger molecules. Therefore, the prefactor N_s proves to be size-independent.

Table IV: Error analyses of partial sRI-CC2 excited gradients among olefin chains (in hartree/bohr).

Molecule	Gradient		S.D.	
	Δ_{max}	$\bar{\Delta}_{abs}$	Δ_{max}	$\bar{\Delta}_{abs}$
C ₂ H ₄	0.0011	0.0004	0.0027	0.0013
C ₄ H ₆	0.0021	0.0005	0.0040	0.0016
C ₆ H ₈	0.0018	0.0004	0.0049	0.0017
C ₈ H ₁₀	0.0022	0.0005	0.0043	0.0016
C ₁₀ H ₁₂	0.0021	0.0005	0.0038	0.0017

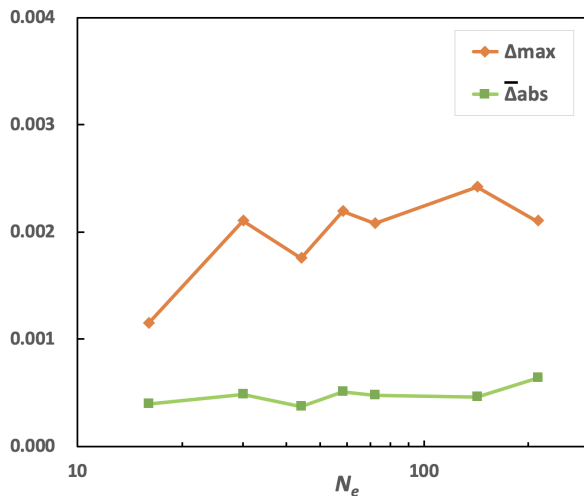


Figure 1: Error analyses among olefin chains.

The CPU time for the gradient calculations of series olefin chains is plotted in Fig. 2. The RI-CC2 scales as $O(N^{4.78})$, while our partial sRI-CC2 as $O(N^{3.94})$. The crossover is predicted to occur approximately at $x = 400$. Our calculations were terminated near $x = 200$ due to the limitation of compute resources. The RI-CC2 formulation remains advantageous for smaller systems (left of the crossover), while the partial sRI-CC2 method demonstrates a signif-

icant performance benefit for larger systems due to its reduced scaling.

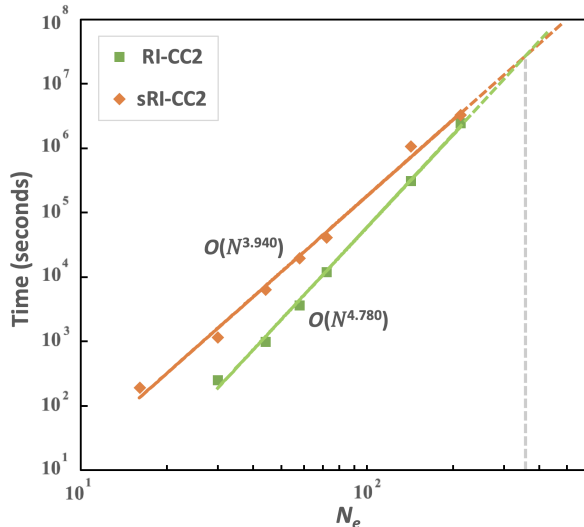


Figure 2: CPU time for calculations of series olefin chains gradient.

B. CC2 derivative coupling

The evaluation of CC2 derivative coupling follows a protocol analogous to the one employed for CC2 gradient. For benchmark references, two established implementations (CCSD and CC2)^[52,84] based on the CFOUR and e^T program systems, respectively,^[85,86] are in developmental versions and inaccessible. Consequently, the performance of our sRI-CC2 implementation is preliminarily assessed against CIS results in Q-Chem^[87] and a CCS implementation by ourselves.

Due to the non-Hermitian of CC2 Jacobian, the absolute value of derivative coupling element encounters a small difference if we exchange the right and left excited states. Therefore, we average the element in any comparison involving CIS by

$$\bar{F}_{mn} = \frac{F_{mn} - F_{nm}}{2} \quad (61)$$

The left state m and right one n are configurable in our programs. In this work, we focus on a pair of nondegenerate states characterized by derivative coupling elements of similar order of magnitude.

Our evaluation begins with a water molecule. Table V presents the largest absolute elements computed at the CIS, CCS, and our RI-CC2 levels. The values of \bar{F}_{41} is too small, so we only focus on the performance in \bar{F}_{21} , \bar{F}_{31} and \bar{F}_{51} . The two rightmost columns give the relative values with respect to CIS results. With the CIS results as the references, the error assessment is

provided in another manner in Table VI with the two measures, Δ_{max} and $\bar{\Delta}_{abs}$. The CCS results fit well with the CIS ones. The RI-CC2 only shows a small difference in the cases of \bar{F}_{31} and \bar{F}_{41} , while the \bar{F}_{21} occurs a large error ($\bar{\Delta}_{abs} = 0.1912$). We attribute this discrepancy to differences between CIS and CC2 in the excited-state amplitude and energy. To test this hypothesis, we performed a hybrid calculation: the excited-state energy was first converged using CCS, and the derivative coupling was subsequently computed using the CC2 code. The results are presented in the row, labeled with ‘CCS→CC2’ in the tables, and show markedly improved agreement with the CIS or CCS values. These evaluations indicate that the error of our CC2 derivative coupling is manageable in certain cases; however, additional tests are still needed to validate its accuracy.

Table V: Derivative coupling element of H₂O (in 1/bohr). In the third and fourth columns, we only list the first and second largest values of derivative coupling matrix for comparison. The last two columns show the relative values compared with CIS. ‘CCS→CC2’ means using the CCS amplitudes in CC2 derivative coupling programs.

Item	Method	Abs largest element		Abs relative value	
		1	2	1	2
\bar{F}_{21}	CIS	2.1581	1.1821	0.0000	0.0000
	CCS	2.1445	1.1753	0.0136	0.0069
	CC2	1.5280	0.8700	0.6301	0.3121
	CCS→CC2	2.1693	1.1894	0.0112	0.0073
\bar{F}_{31}	CIS	0.9327	0.4546	0.0000	0.0000
	CCS	0.9328	0.4546	0.0001	0.0000
	CC2	0.9456	0.4500	0.0129	0.0045
\bar{F}_{51}	CIS	0.3391		0.0000	
	CCS	0.3390		0.0001	
	CC2	0.3382		0.0009	

Taking the RI-CC2 as the reference, we demonstrate the data from partial sRI-CC2 and complete sRI-CC2 in Table VII. Analogous to CC2 gradient, the latter shows larger errors, while the former reproduces the results of RI-CC2 with adjustable stochastic deviations. Besides, the $\bar{\Delta}_{abs}$ for F_{21} is several times greater than the values of F_{31} , consistent with the multiple relation of the largest absolute elements in Table V. This observation underscores the importance of benchmarking on systems with coupling elements of comparable magnitude. More partial sRI-CC2 results are given in Table VIII.

The computational cost of partial sRI-CC2 derivative coupling is assessed on the F_{21} among series (all- E)-olefin chains in Table IX and Fig. 3. The first row for ethylene shows obvious errors due to its large absolute element and the subsequent series return to normal. Still, the statistical error is independent of the system size. Such a result is predictable since the formulation of CC2 derivative

Table VI: Derivative coupling error analyses of H₂O (in 1/bohr). The statistical error takes CIS data as a reference.

Item	Method	Δ_{max}	$\bar{\Delta}_{abs}$
\bar{F}_{21}	CCS	0.0136	0.0042
	CC2	0.6301	0.1912
	CCS→CC2	0.0253	0.0074
\bar{F}_{31}	CCS	0.0001	0.0000
	CC2	0.0128	0.0024
\bar{F}_{51}	CCS	0.0001	0.0000
	CC2	0.0009	0.0002

Table VII: CC2 derivative coupling error analyses of H₂O (in 1/bohr). The statistical error takes RI-CC2 data as a reference.

Item	Partial sRI-CC2				Complete sRI-CC2			
	Derivative coupling		S.D.		Derivative coupling		S.D.	
	Δ_{max}	$\bar{\Delta}_{abs}$	Δ_{max}	$\bar{\Delta}_{abs}$	Δ_{max}	$\bar{\Delta}_{abs}$	Δ_{max}	$\bar{\Delta}_{abs}$
F_{21}	0.0164	0.0076	0.0334	0.0180	0.0767	0.0277	0.1857	0.1368
F_{31}	0.0069	0.0036	0.0280	0.0195	0.0137	0.0078	0.0546	0.0370
F_{51}	0.0026	0.0009	0.0063	0.0043	0.0072	0.0033	0.0189	0.0120

Table VIII: Partial sRI-CC2 derivative coupling error analyses of various systems (in 1/bohr). The error takes RI-CC2 data as a reference.

Molecule	Item	Derivative coupling		S.D.	
		Δ_{max}	$\bar{\Delta}_{abs}$	Δ_{max}	$\bar{\Delta}_{abs}$
LiH	F_{21}	0.0146	0.0087	0.0777	0.0288
HCHO	F_{21}	0.0054	0.0015	0.0098	0.0049
Benzene	F_{21}	0.0209	0.0030	0.0283	0.0098
Furan	F_{32}	0.0522	0.0174	0.1717	0.0667
Pyrrole	F_{21}	0.0518	0.0123	0.2995	0.0916
Pyridine	F_{21}	0.0864	0.0256	0.2984	0.0839

coupling is similar to those of gradient. The error is relatively steady with the increase of system scale and the scaling reduction highlights the performance of sRI in large molecules.

Table IX: Error analyses of partial sRI-CC2 derivative coupling F_{21} among serial olefin chains (in 1/bohr).

Molecule	Derivative coupling		S.D.	
	Δ_{max}	$\bar{\Delta}_{abs}$	Δ_{max}	$\bar{\Delta}_{abs}$
C ₂ H ₄	0.0732	0.0207	0.1476	0.0746
C ₄ H ₆	0.0127	0.0032	0.0178	0.0076
C ₆ H ₈	0.0157	0.0042	0.0206	0.0073
C ₈ H ₁₀	0.0218	0.0030	0.0347	0.0076
C ₁₀ H ₁₂	0.0164	0.0020	0.0297	0.0072

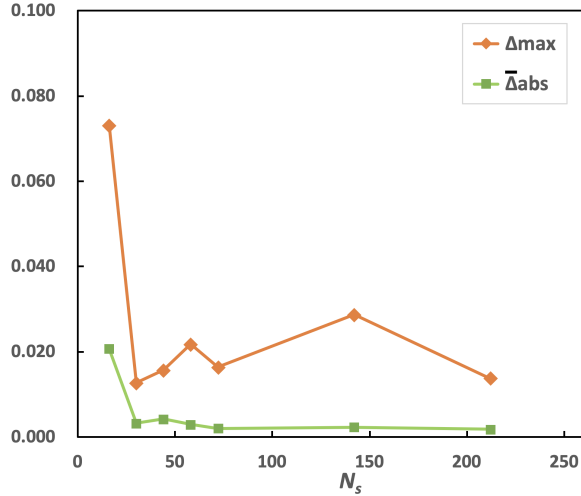


Figure 3: Error analyses among olefin chains.

Again, we present the time consumption for various olefin chains in Fig. 4. The scaling for RI-CC2 is $O(N^{4.41})$, slightly better than $O(N^5)$. And the computational cost for partial sRI-CC2 is $O(N^{3.63})$, in agreement with its theoretical scaling $O(N^4)$. The two plots intersect at about $x = 400$, beyond which the performance of the partial sRI-CC2 method surpasses that of the RI-CC2 approach. For larger systems, our partial sRI-CC2 method presents a computationally feasible alternative.

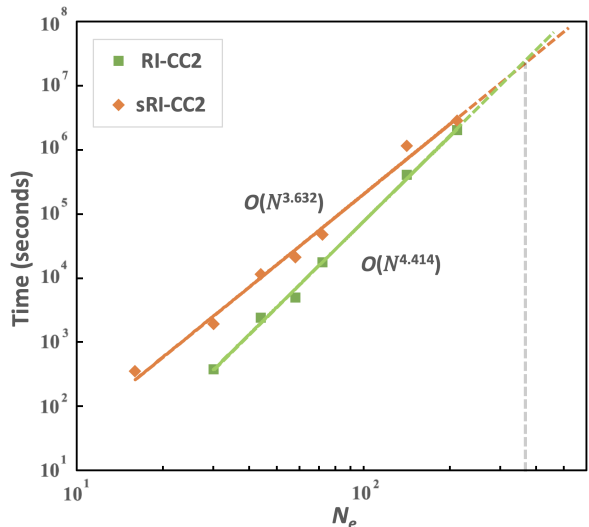


Figure 4: CPU time for calculations of series olefin chains derivative coupling F_{21} .

C. Assessment of the number of stochastic orbitals

In this section, we outline the procedures for selecting an optimal number of stochastic orbitals by evaluating the numerical error across a range of N_s values. In Figs. 5 and 6, we respectively measure the CC2 gradient and derivative coupling of a water molecule. With RI-CC2 as the reference, the left subfigure is for partial sRI-CC2 and the right one for complete sRI-CC2. We notice that all curves decrease sharply with the increase of N_s , then tend to be flat, and will eventually converge to zero at large N_s in theory. A large N_s leads to a smaller stochastic error, but also introduces a large prefactor. For a compromise between accuracy and cost, we adopt the N_s near the turning point among our tests, $N_s = 100$ for partial sRI-CC2 and $N_s = 50000$ for complete sRI-CC2. Beyond these points, the marginal gain in accuracy may be outweighed by the substantial increase in computational cost.

IV. CONCLUSIONS

In this paper, we apply sRI approximation to CC2 model for the efficient calculations of excited-state analytical gradient and derivative coupling. While a full sRI implementation reduces the formal computational scaling from $O(N^5)$ to $O(N^3)$, it introduces a large standard noise. To mitigate this, we introduce a modified approach that applies the sRI approximation selectively to the exchange term. This hybrid scheme achieves an $O(N^4)$ scaling with markedly improved accuracy. The sRI-CC2 is particularly advantageous for large molecular systems with hundreds or even thousands of electrons.

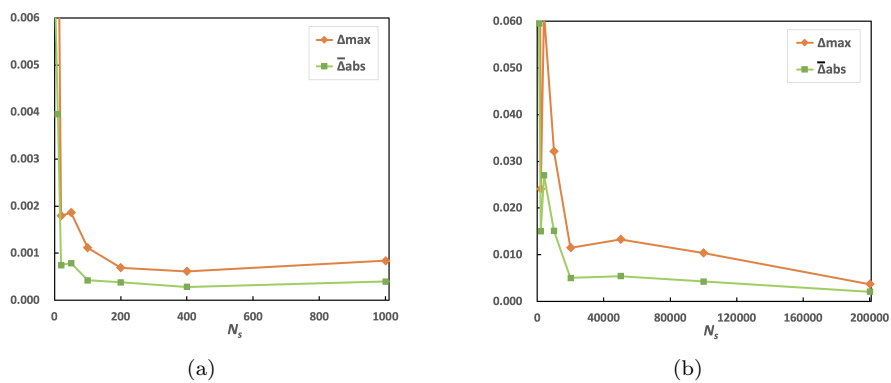


Figure 5: Analytical gradient statistical error for H₂O under different number of stochastic orbitals. The left subfigure is from partial sRI-CC2 and the right one from complete sRI-CC2.

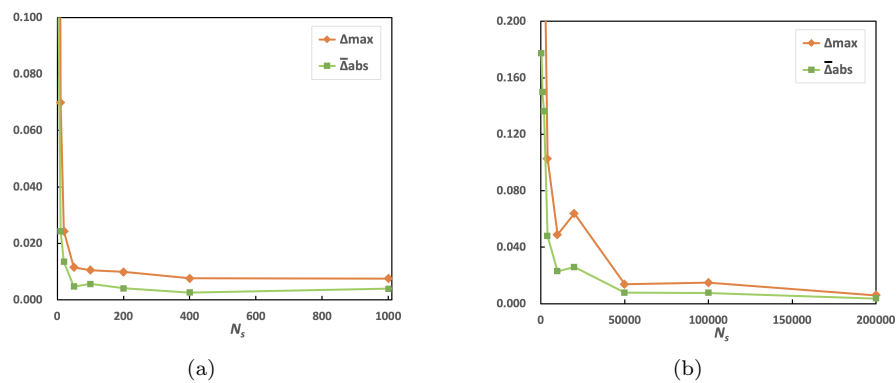


Figure 6: Derivative coupling statistical error for the F_{21} of H₂O under different number of stochastic orbitals. The left subfigure is from partial sRI-CC2 and the right one from complete sRI-CC2.

The present work constitutes a crucial advancement within our developing sRI-CC2 framework. A primary direction for future research involves extending the sRI formalism to the SCC2 method to calculate conical intersections and realize large-scale dynamic simulations. The integration of a robust electronic structure method with nonadiabatic dynamics protocols^[88] presents a highly promising pathway.

AUTHOR DECLARATIONS

Conflict of Interest

The authors have no conflicts to disclose.

ACKNOWLEDGEMENTS

We acknowledge the high-performance computing (HPC) service from Westlake University. W.D. thanks the funding from National Natural Science Foundation of China (No. 22361142829) and Zhejiang Provincial Natural Science Foundation (No. XHD24B0301). C. L. acknowledges the financial support from the National Natural Science Foundation of China (Nos. 22233001, 22473013) and the Fundamental Research Funds for the Central Universities. We are grateful for helpful discussions from Fan Wang, Joonho Lee and Qi Ou.

DATA AVAILABILITY

The data that support the findings of this study are available within the article.

APPENDIX

From Eqs. (18) and (33), a notable difference of one- and two-RDMs for CC2 excited gradient and derivative coupling, compared to those of ground-state gradient, is the *LAR* constraint. The explicit expressions for the additional contributions to these RDMs are provided below. For the case of CC2 derivative coupling, the l_μ is replaced with $\bar{\gamma}_\mu$.

References

- [1] R. Ahlrichs and W. Kutzelnigg, "Direct calculation of approximate natural orbitals and natural expansion coefficients of atomic and molecular electronic wavefunctions. ii. decoupling of the pair equations and calculation of the pair correlation energies for the be and lih ground states," *The Journal of Chemical Physics*, vol. 48, no. 4, pp. 1819–1832, 1968.

Table X: Explicit expressions for RDMs.

$\bar{\gamma}_{ji} \leftarrow -\sum_a l_{ai} r_{aj}$	$\bar{\gamma}_{ab} \leftarrow \sum_i l_{ai} r_{bi}$	$\equiv \bar{\gamma}_{pq}^0$
$\bar{\gamma}_{jb} \leftarrow -\sum_{ai} (l_{ai} r_{aj} t_{bi} + l_{ai} r_{bi} t_{aj})$	$\bar{\gamma}_{jb} \leftarrow \sum_{ai} l_{ai} \hat{r}_{ij}^{ab}$	
$\bar{\gamma}_{bc} \leftarrow \sum_{aij} \hat{l}_{ij}^{ab} r_{ij}^{ac}$	$\bar{\gamma}_{ki} \leftarrow -\sum_{abj} \hat{l}_{ij}^{ab} r_{kj}^{ab}$	
$\bar{\gamma}_{ql}^{pk} \leftarrow \bar{\gamma}_{pq}^0 I_{kl}$	$\bar{\gamma}_{qk}^{pc} \leftarrow \bar{\gamma}_{pq}^0 t_{ck}$	
$\bar{\gamma}_{jl}^{bd} \leftarrow \sum_{ai} l_{ai} r_{bj} \hat{t}_{li}^{da}$	$\bar{\gamma}_{kj}^{cd} \leftarrow -\sum_{ai} l_{ai} r_{aj} t_{ki}^{cd}$	$\bar{\gamma}_{kl}^{cb} \leftarrow -\sum_{ai} l_{ai} r_{bi} t_{kl}^{ca}$
$\bar{\gamma}_{bl}^{ck} \leftarrow \sum_{aij} \hat{l}_{ij}^{ab} r_{ij}^{ac} I_{kl}$	$\bar{\gamma}_{kn}^{im} \leftarrow -\sum_{abj} \hat{l}_{ij}^{ab} r_{kj}^{ab} I_{mn}$	
$\bar{\gamma}_{jq}^{bs} \leftarrow \sum_{ai} l_{ai} r_{bj} \Lambda_{aq}^p \Lambda_{is}^h$	$\bar{\gamma}_{kj}^{bs} \leftarrow -\sum_{ai} l_{ai} r_{kj}^{ba} \Lambda_{is}^h$	$\bar{\gamma}_{pj}^{bc} \leftarrow \sum_{ai} l_{ai} r_{ij}^{bc} \Lambda_{ap}^p$
$\bar{\gamma}_{pq}^{cs} \leftarrow \sum_{aibj} l_{ij}^{ab} r_{ci} \Lambda_{ap}^p \Lambda_{bq}^p \Lambda_{js}^h$	$\bar{\gamma}_{kq}^{rs} \leftarrow -\sum_{ai} l_{ij}^{ab} r_{ak} \Lambda_{bq}^p \Lambda_{ir}^h \Lambda_{js}^h$	

- [2] F. Neese, A. Hansen, and D. G. Liakos, “Efficient and accurate approximations to the local coupled cluster singles doubles method using a truncated pair natural orbital basis,” *The Journal of chemical physics*, vol. 131, no. 6, 2009.
- [3] B. Helmich and C. Hättig, “Local pair natural orbitals for excited states,” *The Journal of chemical physics*, vol. 135, no. 21, 2011.
- [4] B. Helmich and C. Haettig, “A pair natural orbital implementation of the coupled cluster model cc2 for excitation energies,” *The Journal of Chemical Physics*, vol. 139, no. 8, 2013.
- [5] G. Schmitz, C. Hättig, and D. P. Tew, “Explicitly correlated pno-mp2 and pno-ccsd and their application to the s66 set and large molecular systems,” *Physical Chemistry Chemical Physics*, vol. 16, no. 40, pp. 22 167–22 178, 2014.
- [6] P. Pulay, “Localizability of dynamic electron correlation,” *Chemical physics letters*, vol. 100, no. 2, pp. 151–154, 1983.
- [7] C. Hampel and H.-J. Werner, “Local treatment of electron correlation in coupled cluster theory,” *The Journal of chemical physics*, vol. 104, no. 16, pp. 6286–6297, 1996.
- [8] M. Schütz and H.-J. Werner, “Low-order scaling local electron correlation methods. iv. linear scaling local coupled-cluster (lccsd),” *The Journal of Chemical Physics*, vol. 114, no. 2, pp. 661–681, 2001.
- [9] D. Kats, T. Korona, and M. Schütz, “Local cc2 electronic excitation energies for large molecules with density fitting,” *The Journal of chemical physics*, vol. 125, no. 10, 2006.
- [10] J. Gray and S. Kourtis, “Hyper-optimized tensor network contraction,” *Quantum*, vol. 5, p. 410, 2021.

- [11] E. G. Hohenstein, R. M. Parrish, and T. J. Martínez, “Tensor hypercontraction density fitting. i. quartic scaling second-and third-order møller-plesset perturbation theory,” *The Journal of chemical physics*, vol. 137, no. 4, 2012.
- [12] E. G. Hohenstein, S. I. Kokkila, R. M. Parrish, and T. J. Martínez, “Quartic scaling second-order approximate coupled cluster singles and doubles via tensor hypercontraction: Thc-cc2,” *The Journal of chemical physics*, vol. 138, no. 12, 2013.
- [13] E. G. Hohenstein, S. I. Kokkila, R. M. Parrish, and T. J. Martínez, “Tensor hypercontraction equation-of-motion second-order approximate coupled cluster: Electronic excitation energies in o (n 4) time,” *The Journal of Physical Chemistry B*, vol. 117, no. 42, pp. 12 972–12 978, 2013.
- [14] F. Sacchetta, F. H. Bangerter, H. Laqua, and C. Ochsenfeld, “Efficient low-scaling calculation of thc-sos-ir-cc2 and thc-sos-adc (2) excitation energies through density-based integral-direct tensor hypercontraction,” *Journal of Chemical Theory and Computation*, vol. 21, no. 10, pp. 5083–5102, 2025.
- [15] J. Lee, D. W. Berry, C. Gidney, W. J. Huggins, J. R. McClean, N. Wiebe, and R. Babbush, “Even more efficient quantum computations of chemistry through tensor hypercontraction,” *PRX Quantum*, vol. 2, no. 3, p. 030305, 2021.
- [16] S. Grimme, “Improved second-order møller–plesset perturbation theory by separate scaling of parallel-and antiparallel-spin pair correlation energies,” *The Journal of chemical physics*, vol. 118, no. 20, pp. 9095–9102, 2003.
- [17] A. Hellweg, S. A. Grün, and C. Hättig, “Benchmarking the performance of spin-component scaled cc2 in ground and electronically excited states,” *Physical Chemistry Chemical Physics*, vol. 10, no. 28, pp. 4119–4127, 2008.
- [18] A. Tajti and P. G. Szalay, “Accuracy of spin-component-scaled cc2 excitation energies and potential energy surfaces,” *Journal of Chemical Theory and Computation*, vol. 15, no. 10, pp. 5523–5531, 2019.
- [19] Y. Jung, R. C. Lochan, A. D. Dutoi, and M. Head-Gordon, “Scaled opposite-spin second order møller–plesset correlation energy: An economical electronic structure method,” *The Journal of chemical physics*, vol. 121, no. 20, pp. 9793–9802, 2004.
- [20] N. O. Winter and C. Hättig, “Scaled opposite-spin cc2 for ground and excited states with fourth order scaling computational costs,” *The Journal of chemical physics*, vol. 134, no. 18, 2011.
- [21] M. Feyereisen, G. Fitzgerald, and A. Komornicki, “Use of approximate integrals in ab initio theory. an application in mp2 energy calculations,” *Chemical physics letters*, vol. 208, no. 5-6, pp. 359–363, 1993.

- [22] K. Eichkorn, O. Treutler, H. Öhm, M. Häser, and R. Ahlrichs, “Auxiliary basis sets to approximate coulomb potentials,” *Chemical physics letters*, vol. 240, no. 4, pp. 283–290, 1995.
- [23] D. E. Bernholdt and R. J. Harrison, “Large-scale correlated electronic structure calculations: the ri-mp2 method on parallel computers,” *Chemical Physics Letters*, vol. 250, no. 5-6, pp. 477–484, 1996.
- [24] J. Almlöf, “Elimination of energy denominators in møller–plesset perturbation theory by a laplace transform approach,” *Chemical physics letters*, vol. 181, no. 4, pp. 319–320, 1991.
- [25] M. Häser and J. Almlöf, “Laplace transform techniques in møller–plesset perturbation theory,” *The Journal of chemical physics*, vol. 96, no. 1, pp. 489–494, 1992.
- [26] M. Häser, “Møller–plesset (mp2) perturbation theory for large molecules,” *Theoretica chimica acta*, vol. 87, pp. 147–173, 1993.
- [27] R. Baer, D. Neuhauser, and E. Rabani, “Self-averaging stochastic kohn–sham density-functional theory,” *Physical review letters*, vol. 111, no. 10, p. 106402, 2013.
- [28] D. Neuhauser, R. Baer, and E. Rabani, “Communication: Embedded fragment stochastic density functional theory,” *The Journal of chemical physics*, vol. 141, no. 4, 2014.
- [29] Y. Gao, D. Neuhauser, R. Baer, and E. Rabani, “Sublinear scaling for time-dependent stochastic density functional theory,” *The Journal of chemical physics*, vol. 142, no. 3, 2015.
- [30] D. Neuhauser, E. Rabani, Y. Cytter, and R. Baer, “Stochastic optimally tuned range-separated hybrid density functional theory,” *The Journal of Physical Chemistry A*, vol. 120, no. 19, pp. 3071–3078, 2016.
- [31] N. C. Bradbury, T. Allen, M. Nguyen, and D. Neuhauser, “Deterministic/fragmented-stochastic exchange for large-scale hybrid dft calculations,” *Journal of Chemical Theory and Computation*, vol. 19, no. 24, pp. 9239–9247, 2023.
- [32] D. Neuhauser, E. Rabani, and R. Baer, “Expeditious stochastic approach for mp2 energies in large electronic systems,” *Journal of Chemical theory and Computation*, vol. 9, no. 1, pp. 24–27, 2013.
- [33] Q. Ge, Y. Gao, R. Baer, E. Rabani, and D. Neuhauser, “A guided stochastic energy-domain formulation of the second order møller–plesset perturbation theory,” *The Journal of Physical Chemistry Letters*, vol. 5, no. 1, pp. 185–189, 2014.

- [34] T. Y. Takeshita, W. A. de Jong, D. Neuhauser, R. Baer, and E. Rabani, “Stochastic formulation of the resolution of identity: Application to second order møller–plesset perturbation theory,” *Journal of Chemical Theory and Computation*, vol. 13, no. 10, pp. 4605–4610, 2017.
- [35] D. Neuhauser, R. Baer, and D. Zgid, “Stochastic self-consistent second-order green’s function method for correlation energies of large electronic systems,” *Journal of chemical theory and computation*, vol. 13, no. 11, pp. 5396–5403, 2017.
- [36] T. Y. Takeshita, W. Dou, D. G. Smith, W. A. de Jong, R. Baer, D. Neuhauser, and E. Rabani, “Stochastic resolution of identity second-order matsubara green’s function theory,” *The Journal of chemical physics*, vol. 151, no. 4, 2019.
- [37] W. Dou, T. Y. Takeshita, M. Chen, R. Baer, D. Neuhauser, and E. Rabani, “Stochastic resolution of identity for real-time second-order green’s function: ionization potential and quasi-particle spectrum,” *Journal of chemical theory and computation*, vol. 15, no. 12, pp. 6703–6711, 2019.
- [38] W. Dou, M. Chen, T. Y. Takeshita, R. Baer, D. Neuhauser, and E. Rabani, “Range-separated stochastic resolution of identity: Formulation and application to second-order green’s function theory,” *The Journal of chemical physics*, vol. 153, no. 7, 2020.
- [39] L. Mejía, S. Sharma, R. Baer, G. K.-L. Chan, and E. Rabani, “Convergence analysis of the stochastic resolution of identity: Comparing hutchinson to hutch++ for the second-order green’s function,” *Journal of Chemical Theory and Computation*, vol. 20, no. 17, pp. 7494–7502, 2024.
- [40] E. Rabani, R. Baer, and D. Neuhauser, “Time-dependent stochastic bethe-salpeter approach,” *Physical Review B*, vol. 91, no. 23, p. 235302, 2015.
- [41] J. Lee and D. R. Reichman, “Stochastic resolution-of-the-identity auxiliary-field quantum monte carlo: Scaling reduction without overhead,” *The Journal of Chemical Physics*, vol. 153, no. 4, 2020.
- [42] C. Zhao, J. Lee, and W. Dou, “Stochastic resolution of identity to cc2 for large systems: Ground state and triplet excitation energy calculations,” *The Journal of Physical Chemistry A*, vol. 128, no. 42, pp. 9302–9310, 2024.
- [43] C. Zhao, Q. Ou, J. Lee, and W. Dou, “Stochastic resolution of identity to cc2 for large systems: excited state properties,” *Journal of Chemical Theory and Computation*, vol. 20, no. 12, pp. 5188–5195, 2024.
- [44] C. Zhao, Q. Ou, C. Li, and W. Dou, “Stochastic resolution of identity to cc2 for large systems: Oscillator strength and ground state gradient calculations,” *The Journal of Chemical Physics*, vol. 163, no. 2, p. 024102, 2025.

- [45] A. Köhn and C. Hättig, “Analytic gradients for excited states in the coupled-cluster model cc2 employing the resolution-of-the-identity approximation,” *The Journal of chemical physics*, vol. 119, no. 10, pp. 5021–5036, 2003.
- [46] N. O. Winter and C. Hättig, “Quartic scaling analytical gradients of scaled opposite-spin cc2,” *Chemical Physics*, vol. 401, pp. 217–227, 2012.
- [47] K. Ledermüller, D. Kats, and M. Schütz, “Local cc2 response method based on the laplace transform: Orbital-relaxed first-order properties for excited states,” *The Journal of Chemical Physics*, vol. 139, no. 8, p. 084111, 2013.
- [48] K. Ledermüller and M. Schütz, “Local cc2 response method based on the laplace transform: analytic energy gradients for ground and excited states,” *The Journal of Chemical Physics*, vol. 140, no. 16, p. 164113, 2014.
- [49] J. Heuser and S. Höfener, “Analytical nuclear excited-state gradients for the second-order approximate coupled-cluster singles and doubles (cc2) method employing uncoupled frozen-density embedding,” *Journal of Chemical Theory and Computation*, vol. 14, no. 9, pp. 4616–4628, 2018.
- [50] C. Hättig, “Structure optimizations for excited states with correlated second-order methods: Cc2 and adc(2),” *Advances in Quantum Chemistry*, vol. 50, pp. 37–60, 2005.
- [51] A. Köhn and A. Tajti, “Can coupled-cluster theory treat conical intersections?” *The Journal of chemical physics*, vol. 127, no. 4, 2007.
- [52] E. F. Kjønstad and H. Koch, “Communication: Non-adiabatic derivative coupling elements for the coupled cluster singles and doubles model,” *The Journal of Chemical Physics*, vol. 158, no. 16, 2023.
- [53] E. F. Kjønstad, S. Angelico, and H. Koch, “Coupled cluster theory for nonadiabatic dynamics: nuclear gradients and nonadiabatic couplings in similarity constrained coupled cluster theory,” *Journal of Chemical Theory and Computation*, vol. 20, no. 16, pp. 7080–7092, 2024.
- [54] L. Stoll, S. Angelico, E. F. Kjønstad, and H. Koch, “Similarity constrained cc2 for efficient coupled cluster nonadiabatic dynamics,” *arXiv preprint arXiv:2504.11157*, 2025.
- [55] E. F. Kjønstad and H. Koch, “Resolving the notorious case of conical intersections for coupled cluster dynamics,” *The Journal of Physical Chemistry Letters*, vol. 8, no. 19, pp. 4801–4807, 2017.
- [56] E. F. Kjønstad and H. Koch, “An orbital invariant similarity constrained coupled cluster model,” *Journal of Chemical Theory and Computation*, vol. 15, no. 10, pp. 5386–5397, 2019.

- [57] F. Rossi, E. F. Kjønstad, S. Angelico, and H. Koch, “Generalized coupled cluster theory for ground and excited state intersections,” *The Journal of Physical Chemistry Letters*, vol. 16, no. 2, pp. 568–578, 2025.
- [58] D. G. Smith, L. A. Burns, A. C. Simmonett, R. M. Parrish, M. C. Schieber, R. Galvelis, P. Kraus, H. Kruse, R. Di Remigio, A. Alenaizan *et al.*, “Psi4 1.4: Open-source software for high-throughput quantum chemistry,” *The Journal of chemical physics*, vol. 152, no. 18, 2020.
- [59] H. Lischka, R. Shepard, T. Müller, P. G. Szalay, R. M. Pitzer, A. J. Aquino, M. M. Araújo do Nascimento, M. Barbatti, L. T. Belcher, J.-P. Blaudeau *et al.*, “The generality of the guga mrci approach in columbus for treating complex quantum chemistry,” *The Journal of Chemical Physics*, vol. 152, no. 13, 2020.
- [60] Q. Sun, X. Zhang, S. Banerjee, P. Bao, M. Barbry, N. S. Blunt, N. A. Bogdanov, G. H. Booth, J. Chen, Z.-H. Cui *et al.*, “Recent developments in the pyscf program package,” *The Journal of chemical physics*, vol. 153, no. 2, 2020.
- [61] E. Epifanovsky, A. T. Gilbert, X. Feng, J. Lee, Y. Mao, N. Mardirossian, P. Pokhilko, A. F. White, M. P. Coons, A. L. Dempwolff *et al.*, “Software for the frontiers of quantum chemistry: An overview of developments in the q-chem 5 package,” *The Journal of chemical physics*, vol. 155, no. 8, 2021.
- [62] G. P. Paran, C. Utku, and T.-C. Jagau, “A spin-flip variant of the second-order approximate coupled-cluster singles and doubles method,” *Physical Chemistry Chemical Physics*, vol. 24, no. 44, pp. 27 146–27 156, 2022.
- [63] G. P. Paran, C. Utku, and T.-C. Jagau, “On the performance of second-order approximate coupled-cluster singles and doubles methods for non-valence anions,” *Physical Chemistry Chemical Physics*, vol. 26, no. 3, pp. 1809–1818, 2024.
- [64] M. Alessio, G. P. Paran, C. Utku, A. Grüneis, and T.-C. Jagau, “Coupled-cluster treatment of complex open-shell systems: the case of single-molecule magnets,” *Physical Chemistry Chemical Physics*, vol. 26, no. 24, pp. 17 028–17 041, 2024.
- [65] O. Christiansen, H. Koch, and P. Jørgensen, “The second-order approximate coupled cluster singles and doubles model cc2,” *Chemical Physics Letters*, vol. 243, no. 5-6, pp. 409–418, 1995.
- [66] H. Sekino and R. J. Bartlett, “A linear response, coupled-cluster theory for excitation energy,” *International Journal of Quantum Chemistry*, vol. 26, no. S18, pp. 255–265, 1984.
- [67] H. Koch and P. Jørgensen, “Coupled cluster response functions,” *Journal of Chemical Physics*, vol. 93, no. 5, pp. 3333–3344, 1990.

- [68] K. Hald, C. Hättig, D. L. Yeager, and P. Jørgensen, “Linear response cc2 triplet excitation energies,” *Chemical Physics Letters*, vol. 328, no. 3, pp. 291–301, 2000.
- [69] J. Geertsen, M. Rittby, and R. J. Bartlett, “The equation-of-motion coupled-cluster method: Excitation energies of be and co,” *Chemical Physics Letters*, vol. 164, no. 1, pp. 57–62, 1989.
- [70] D. C. Comeau and R. J. Bartlett, “The equation-of-motion coupled-cluster method. applications to open-and closed-shell reference states,” *Chemical Physics Letters*, vol. 207, no. 4-6, pp. 414–423, 1993.
- [71] J. F. Stanton and R. J. Bartlett, “The equation of motion coupled-cluster method. a systematic biorthogonal approach to molecular excitation energies, transition probabilities, and excited state properties,” *The Journal of chemical physics*, vol. 98, no. 9, pp. 7029–7039, 1993.
- [72] J. F. Stanton and J. Gauss, “Perturbative treatment of the similarity transformed hamiltonian in equation-of-motion coupled-cluster approximations,” *The Journal of chemical physics*, vol. 103, no. 3, pp. 1064–1076, 1995.
- [73] S. R. Gwaltney, M. Nooijen, and R. J. Bartlett, “Simplified methods for equation-of-motion coupled-cluster excited state calculations,” *Chemical physics letters*, vol. 248, no. 3-4, pp. 189–198, 1996.
- [74] S. Haldar, T. Mukhopadhyay, and A. K. Dutta, “A similarity transformed second-order approximate coupled cluster method for the excited states: Theory, implementation, and benchmark,” *The Journal of Chemical Physics*, vol. 156, no. 1, 2022.
- [75] T. Helgaker and P. Jørgensen, “Analytical calculation of geometrical derivatives in molecular electronic structure theory,” *Advances in quantum chemistry*, vol. 19, pp. 183–245, 1988.
- [76] O. Christiansen, P. Jørgensen, and C. Hättig, “Response functions from fourier component variational perturbation theory applied to a time-averaged quasienergy,” *International Journal of Quantum Chemistry*, vol. 68, no. 1, pp. 1–52, 1998.
- [77] S. V. Levchenko, T. Wang, and A. I. Krylov, “Analytic gradients for the spin-conserving and spin-flipping equation-of-motion coupled-cluster models with single and double substitutions,” *The Journal of chemical physics*, vol. 122, no. 22, 2005.
- [78] X. Feng, E. Epifanovsky, J. Gauss, and A. I. Krylov, “Implementation of analytic gradients for ccSD and eom-ccSD using cholesky decomposition of the electron-repulsion integrals and their derivatives: Theory and benchmarks,” *The Journal of chemical physics*, vol. 151, no. 1, 2019.

- [79] C. Hättig and A. Köhn, “Transition moments and excited-state first-order properties in the coupled-cluster model *cc2* using the resolution-of-the-identity approximation,” *The Journal of chemical physics*, vol. 117, no. 15, pp. 6939–6951, 2002.
- [80] J. Gerratt and I. M. Mills, “Force constants and dipole-moment derivatives of molecules from perturbed hartree–fock calculations. i,” *The Journal of Chemical Physics*, vol. 49, no. 4, pp. 1719–1729, 1968.
- [81] N. C. Handy and H. F. Schaefer III, “On the evaluation of analytic energy derivatives for correlated wave functions,” *The Journal of chemical physics*, vol. 81, no. 11, pp. 5031–5033, 1984.
- [82] O. Christiansen, A. Halkier, H. Koch, P. Jørgensen, and T. Helgaker, “Integral-direct coupled cluster calculations of frequency-dependent polarizabilities, transition probabilities and excited-state properties,” *The Journal of chemical physics*, vol. 108, no. 7, pp. 2801–2816, 1998.
- [83] S. G. Balasubramani, G. P. Chen, S. Coriani, M. Diedenhofen, M. S. Frank, Y. J. Franzke, F. Furche, R. Grotjahn, M. E. Harding, C. Hättig *et al.*, “Turbomole: Modular program suite for ab initio quantum-chemical and condensed-matter simulations,” *The Journal of chemical physics*, vol. 152, no. 18, 2020.
- [84] A. Tajti and P. G. Szalay, “Analytic evaluation of the nonadiabatic coupling vector between excited states using equation-of-motion coupled-cluster theory,” *The Journal of chemical physics*, vol. 131, no. 12, 2009.
- [85] D. A. Matthews, L. Cheng, M. E. Harding, F. Lipparini, S. Stopkowicz, T.-C. Jagau, P. G. Szalay, J. Gauss, and J. F. Stanton, “Coupled-cluster techniques for computational chemistry: The *cfour* program package,” *The Journal of Chemical Physics*, vol. 152, no. 21, 2020.
- [86] S. D. Folkestad, E. F. Kjørstad, R. H. Myhre, J. H. Andersen, A. Balbi, S. Coriani, T. Giovannini, L. Goletto, T. S. Haugland, A. Hutcheson *et al.*, “*et* 1.0: An open source electronic structure program with emphasis on coupled cluster and multilevel methods,” *The Journal of Chemical Physics*, vol. 152, no. 18, 2020.
- [87] S. Fatehi, E. Alguire, Y. Shao, and J. E. Subotnik, “Analytic derivative couplings between configuration-interaction-singles states with built-in electron-translation factors for translational invariance,” *The Journal of chemical physics*, vol. 135, no. 23, 2011.
- [88] W. Liu, R.-H. Bi, and W. Dou, “Scalable neural quantum state based kernel polynomial method for optical properties from the first principle,” *arXiv preprint arXiv:2506.07430*, 2025.